EXPLICIT NUMERICAL SIMULATION OF CUMULUS
WITHIN A DEVELOPING TROPICAL CYCLONE

by Gregory J. Tripoli
University of Wisconsin-Madison
Madison, Wisconsin

# 1. Introduction

In recent years, it has become practical to perform simulations of convective systems for which the cumulus are explicitly resolved rather than parameterized. Analysis of the simulated statistical impact of the cumulus population on the system and of the system on the cumulus highlight probable mechanisms of cumulus-system interaction which are consistent with the physics and numerics of the model and presumably consistent with observed atmospheric processes. In this paper, we present a numerical simulation of a developing tropical wave observed during the TEXMEX field experiment held in the Eastern Pacific during the summer of 1991. The case is interesting because the observed convective system struggled to develop briefly into a category 1 cyclone. In doing so, the system passed through three phases of cumulus activity including pre- genesis, genesis, and post genesis phases. It is instructive to study how the statistical characteristics of the scale interaction change throughout the genesis process.

The simulation was of the genesis of tropical cyclone Fefa in the northeast pacific on 28-31 August, 1991. The results suggested that the genesis represented a transition phase from an initial grouping of transient convective entities to an organized growing and inertially balanced flow system which efficiently utilized the latent heat energy absorbed from the sea and transferred into the mid to upper troposphere. Early pre-genesis organization of the transients was apparently coupled to a tropospheric maximum of diabatically generated potential vorticity. During genesis the potential vorticity center continued to act as a focal point for continued growth and remained the focal point of the circulation into the deepening and maturing phases of the storm.

Numerical sensitivity tests suggested that the transition was initiated by changing atmospheric structure along the path of the storm resulting from the influence of the Sierra-Madre Mountains to the east of the genesis area. In other words evolution of the statistically averaged

heating and moistening profiles by the convection was less at issue than was the evolution of the mesoscale dynamical environment with which they interacted. In this paper, the statistical mean heating, moistening and potential vorticity forcings on the meso-$\beta$ scale defined by the mean forcing across a selected circular region 200 km in diameter centered on the cluster will be examined. Apparent heat and moisture sources will be partitioned between the moist, radiative and cumulus transport. Moist adiabatic heating will be partitioned into the contributions from the different phase transitions between ice, liquid and vapor. In section 3, the statistical evolution of potential vorticity and the relative importance of each generation mechanism will be examined. Finally, conclusions concerning the implications of these results on cumulus parameterization will be discusses in section 4.

## 2. Summary of Experiment Design

The outer grid chosen spanned 60 degrees of latitude centered at 10 N and 75 degrees of longitude centered at 107.5 W. Its spacing was 2.5 degrees latitude by 2.5 degrees longitude, in accordance with the archived ECMWF data set used to force the initial and boundary conditions. This grid was chosen to capture the equatorward position of the middle latitude baroclinic forcing. Much of that forcing was ultimately controlled by the boundary forcing, which was derived from the synoptic analyses used to initiate the simulation and subsequent analyses used and the time-varying boundary conditions. The vertical resolution for this and all inner grids was 200m near the surface expanding to 800 m at upper levels. A total of 39 levels were used reaching up to 25 km elevation.

The movable medium grid was set along the ITCZ to track the easterly wave in which Fefa developed. A 5:1 grid spacing reduction from grid 1 provided 0.5 degree ( about 55 km) resolution in grid 2. Grid 2, with 82 by 42 grid boxes spanned 40 degrees longitude by 20 degrees latitude and spanned the track which Fefa followed for the 3.5 day period of the simulation. The effects of cumulus convection were parameterized on grids 1 and 2 using a modified form of the Emanuel (1992) cumulus parameterization.

A movable fine grid of 0.1 degree resolution and spanning 660 km was added after 12 hours of integration and centered over the circulation center of the wave. The track of the circulation center was diagnosed from several preliminary 2-grid runs of the experiment. Initial tests were conducted with a larger 11 km third grid, but results suggested that the region of

active convection was limited enough that a smaller and more economical third grid could be employed, allowing resources to be diverted to a fourth cloud-resolving grid.

A movable extra-fine mesh (4th grid) was centered over the region of active genesis and added after 24 hours of integration. The grid spacing selected was 0.033 degrees or about 3.7 km. The span of the extra fine mesh was 370 km on a side. Although small, this was sufficient to capture the core of the convection associated with genesis. Convection was explicit in both the third and fourth grids and cumulus parameterization was turned off.

The numerical model employed was the University of Wisconsin Nonhydrostatic Modeling System (UW-NMS). This is a quasi-compressible non-Boussinesq cloud/mesoscale model designed originally to simulate convective storms (Cotton et al., 1982) and later extended to also simulate scale interaction on the meso and synoptic scale (?; Tripoli, 1993). Cloud-active radiation (Chen and Cotton, 1983) and a surface layer were employed over a soil (Tremback and Kessler, 1985) or ocean surface. The vertical coordinate was height with step topography (Tripoli, 1994). The 1.5 level turbulence closure, employing a predictive variable for moist turbulent kinetic energy (Tripoli, 1992) was employed in the vertical while deformation based nonlinear diffusion was used in the horizontal. An additional weak 6th order numerical filter was employed in the vertical and an additional weak 4th order numerical filter was employed in the horizontal to suppress numerical aliasing.

The microphysics model options activated were cloud water, rain, pristine crystals, snow aggregates, and graupel. Pristine crystals were assumed to be of a constant mass of $1.5x10^{-6}$ grams in order to maintain a differentiation between mature crystals and newly nucleated pristine crystals. In the absence of sufficient resolution to resolve the internal microphysical interactions within cumulus, this method was chosen to maintain reasonable anvils based on two dimensional experiments with high resolution and fully explicit ice growth in all categories.

The initial state at 00 UTC July 28, 1991 and subsequent analyzed states at 12 hour intervals of potential temperature, pressure, moisture, and horizontal wind were interpolated from the ECMWF analyses directly to the model grid. The interpolated fields were rebalanced only hydrostatically. The interpolated ECMWF analysis was used not only for the initial state, but as a lateral and upper boundary condition to subsequent states. These boundary conditions were applied through a 4 point rayleigh damping zone at the lateral and upper model boundaries. The lateral boundaries additionally employed the Klemp and Lilly (1980) radiation condition to allow fast outward propagating waves to pass out of the domain.

The experiment was run over several grid configurations and initialization data sets to reach a finalized design which captured genesis. Several cumulus parameterizations were attempted with the two grid simulations to capture genesis including a Modified Kuo scheme (Cotton and Tremback, 1989), the Kain and Fritsch scheme, the Emanuel(1991) scheme and finally the modified Emanuel (1991) scheme. Initial tests of the Kuo scheme resulted in the production of false tropical cyclones forming due to a tendency for the scheme to grow any cumulus cluster into a cyclone. Tests with the Kain and Fritsch scheme failed because that scheme tended to too easily deepen the developing storm into the westerly flow aloft, leading to recurvature to the northeast from its observed eastward path. The Emanuel (1991) scheme, was unsuccessful in placing convection preferentially within the wave, instead producing unfocused wide spread convection without strong ties to model prescribed forcing or suppression. Nevertheless, we did find the scheme to perform well by creating realistic vertical moistening and heating profiles. As a result, the author revised the convective forcing mechanisms of the Emanuel scheme to be enhance convection where modeled mesoscale vertical motion was supportive and where local downdrafts produced by convection fed back into new updraft development. The improvements also caused the scheme to suppress convection where the modeled mesoscale vertical motion was not supportive . Calculated convective updraft coverage and downdraft coverage was redesigned to respond to the mesoscale forcings in a way quantitatively similar to that indicated by our explicit modeling results of convection. The result was a more successful parameterization which did not produce false storms as did the Kuo, did not produce false movement as did the Kain and Fritsch and did model what seemed to be an appropriate response to the forcing of the easterly wave. In addition the superior heating and moistening profiles of the Emanuel scheme were preserved. The modifications to the Emanuel scheme have been tested and compared to the other schemes by other investigators in a wide variety of middle latitude and convective environments with similar successes. We will report on the exact nature of our modifications to the Emanuel scheme at a later date.

In this paper we will discuss some ensemble characteristics of the convection modeled explicitly within the fourth extra fine mesh grid where, along with the third fine mesh grid, the parameterization was turned off. It should be noted that simulations run with only the two outer grids and relying totally on the modified Emanuel cumulus parameterization did perform well in simulating the time and location of storm growth, but were not able to capture the full strength of the strom because of the coarse 55 km mesh. This is significant because it

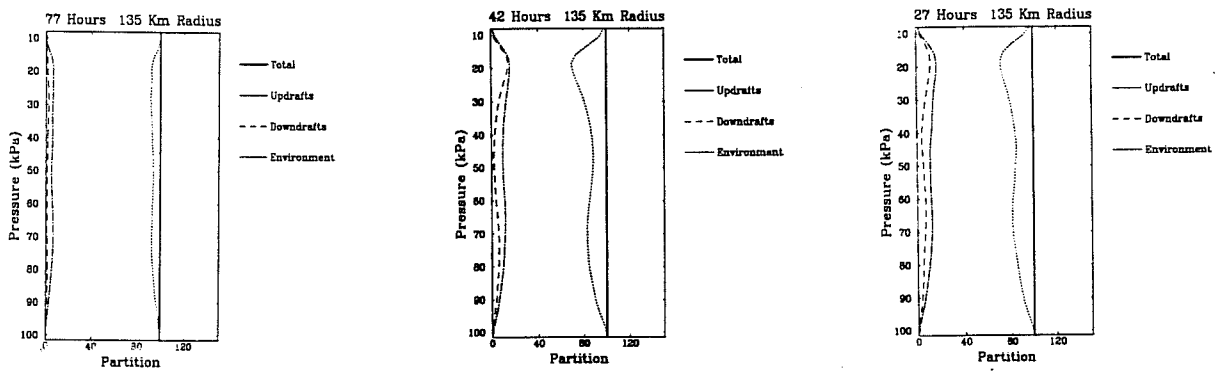


Figure 1: Graph of percentage of area occupied by updrafts, downdrafts, and environment outside of the convection. The threshold vertical velocity defining an updraft is 1 m/s and that defining a downdraft is -1 m/s.

suggests a strong role of the large scale to determining the timing and location of genesis.

# 3. Vertical Mass Flux in Storm Core

It is first useful to view how the domain of Grid 4 is partitioned between updrafts, downdrafts and environment. To do so we institute an averaging procedure with respect to the inner or 4th Grid of the simulation. The averaging procedure was the simple density weighted area average. In order to determine how the averaged variable is partitioned among convective updrafts, downdrafts and the static environment, the averaged variables were also averaged over the updraft area defined as grid boxes with upward vertical motion in excess of 1 $ms^{-1}$ and downdraft defined as grid boxes with vertical motion less than -1 $ms^{-1}$ and the environment around these areas. Each partitions contribution was divided by the total area so that the sum of the three partitions equals the total average of the variable. The resulting vertical profiles were then weighted by density and plotted on a vertical pressure scale.

Figure 1 displays the partitioning as a percent of the total area at 3 model times of 29, 42, and 77 hours of integration. 27 hours was chosen to represent the environment just before genesis and sufficiently after initialization of the fourth grid to develop an approximate steadiness to the cloud field. 42 hours represents the time of transition to the deepening stage while 77 hours represents the late stages of mature stage where there is already some evidence of storm weakening. Note that in each case The updrafts and downdrafts combined occupy

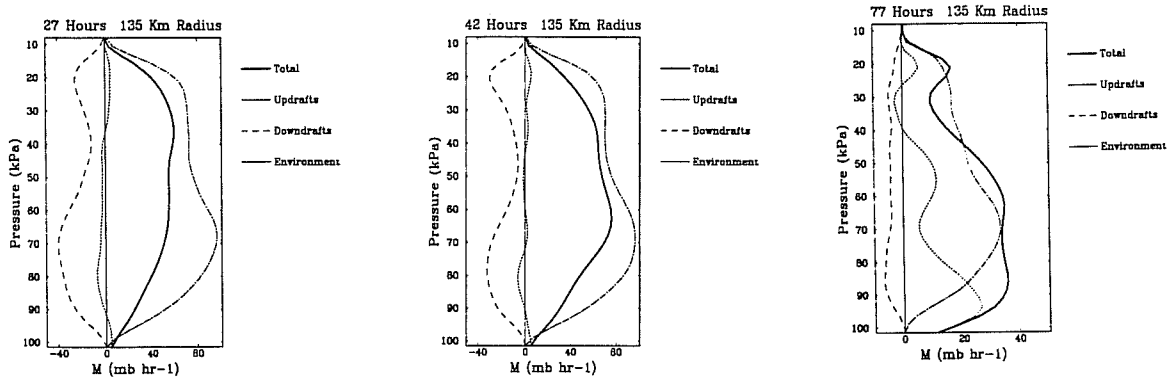


Figure 2: Mean upward mass flux for the three time periods used in figure 1

less than 10generally that percentage stays approximately constant until the dissipation stage.

The total upward mass flux expressed in $mmhr^{-1}$ associated with each of these areas is given by:

$$M = \rho_o g u_3 \tag{1}$$

where $g$ is the gravity acceleration. Figure 2 displays how the domain mean $M$ is partitioned with respect to the cumulus plumes. Note that the peak levels of mean upward mass flux varies considerably dependent on the degree of overall convective activity. Note also that the mean vertical mass flux is most strongly controlled by the contribution of the cumulus updrafts, except during the dissipating stages of the cyclone. Also note that during these periods, there tends to be some tendency for the small amount of mass flux of the environment and the downdrafts to cancel. Together, this paints a picture of a domain with a mean upward mass flux realized as locally uncompensated cumulus drafts, the compensation being largely confined to outside the domain.

# 4. Heat and Moisture Budgets due to Convection

The local change in dry static energy, expressed as a change in potential temperature, may be written as:

$$\frac{\partial \theta}{\partial t} - \frac{1}{\rho_o}\left(\frac{\partial \rho_o u_i \theta}{\partial x_i}\right)_{i=1,2} - \frac{1}{\rho_o}\frac{\partial \rho_o \overline{u_3}\,\overline{\theta}}{\partial x_3} = -\frac{1}{\rho_o}\frac{\partial u_3' \theta'}{\partial x_3} + \left(\frac{L_{vl}}{\pi}\frac{r_l}{dt} + \frac{L_{iv}}{\pi}\frac{d_i r_i}{dt}\right) + Q_R = Q1 \tag{2}$$

where $\theta$ is potential temperature, $r_l$ is the mixing ratio of liquid water, $r_i$ is the mixing

ratio of ice, $\rho_o$ is the reference state moist air density, $\pi$ is the exner function, $u_i$ is the ith component of motion in a Cartesian system where the 3rd component points up vertically, $x_i$ is the Cartesian vector in the ith direction and t is time. The internal derivatives are subscripted with "i" and represent adiabatic changes in phase. Hence :

$$dr_v + d_i r_l + d_i r_i = 0 \tag{3}$$

where $r_v$ is the vapor mixing ratio. The barred quantities represent horizontal means taken across the fine mesh domain and the primed quantities are deviations from that mean. $Q_R$ represents the tendency of potential temperature due to radiative transfer. $L_{vl}$ and $L_{vi}$ represent the latent heats of condensation and sublimation respectively.

The right hand side represents the net effect of the convective scale fluctuations relative to the mean vertical transport and radiative transfer over the 4th grid and is appropriately expressed as the apparent moisture source $Q1$. The arbitrary scale separation is made with respect to an averaging scale defined by the scale of the 4th grid domain which is 370 km or approximately a minimal meso-$\alpha$ scale. $Q1 - QR$ would isolate the convective scale (meso-$\beta$ scale and smaller) effects on heating together with the total condensation which may contain both meso-$\alpha$ and meso-$\beta$ scale contributions.

The moisture continuity equation, can be similarly be partitioned and expressed in terms of an apparent heat sink ($Q2$) as:

$$-\frac{L_{vl}}{\pi}\left(\frac{\partial r_v}{\partial t}+\frac{1}{\rho_o}\frac{\partial \rho_o u_i r_v}{\partial x_i}\right)_{i=1,2}=\frac{1}{\rho_o}\left(\frac{\partial \rho_o \overline{u_3 r_v}}{\partial x_3}\right)=-\frac{L_v l}{\pi}\left(-\frac{1}{\rho_o}\frac{\partial u_3' r_v'}{\partial x_3}\right)+\frac{L_{vl}}{\pi}\left(\frac{d_i r_l}{dt}+\frac{d_i r_l}{dt}\right)=Q2. \tag{4}$$

Note here that in order to be consistent with traditional formulations of moist static energy, the latent heat of condensation is used for the latent energy contributed by the water vapor. Hence the change in moist static energy due to convective motions, radiation and phase changes is approximately $Q1 - Q2$.

These terms were computed and then averaged over the domain to determine their mean impact to the meso-$\alpha$ scale. Hence this partitioning effectively depicts the contributions to the total heating process by updraft, downdraft and environment of the convection.

Figure 3 depicts Q1 as it is partitioned over the 3 time periods of analysis. Note that in each case, Q1 receives its major contribution from the region between the updrafts and downdrafts called the environment. The vertical level of peak heating is found to be 300-500

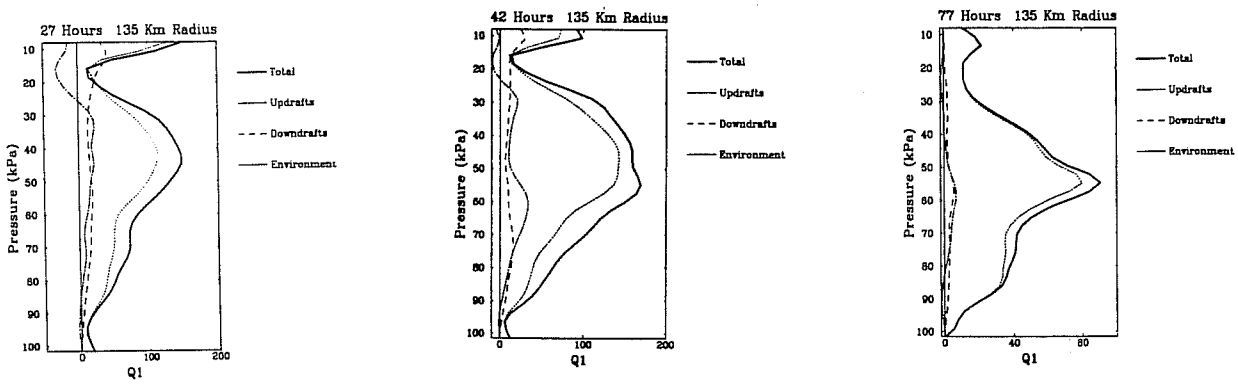


Figure 3: Q1 heating for three time periods used in figure 1

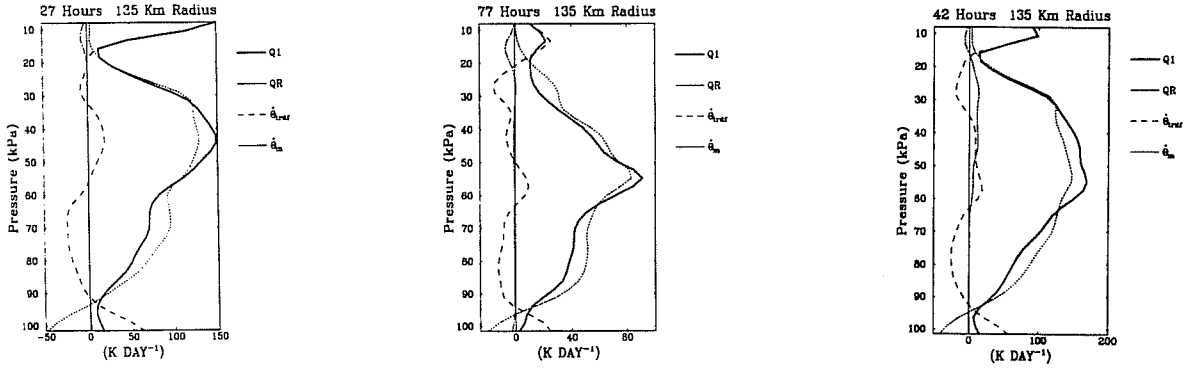


Figure 4: Same as figure 3 except Q1 is partitioned into contributions by radiative transfer (QR), transport and phase changes.

mb early, but migrates downward to near 500 mb later. This level has the significance of being the melting level for ice. It is interesting that the updrafts, although containing the major portion of the vertical mass flux have little net impact on Q1.

Figure 4 breaks Q1 into its components of QR, transport and diffusion and internal phase changes. Notice that phase changes dominate all contributions to Q1 while convective scale transport or radiation have little effect. This may seem contradictory in view of the fact that the net effect of Q1 is produced in the environment rather than in the updraft where the phase changes are occurring. The simple explanation for this paradox is that the heating from moistening in the updraft is largely canceled by the cooling due to moist ascent. In fact, figure 4 shows contribution from Q1 to literally vanish within the updrafts suggesting steady moist adiabatic neutral ascent within the updrafts.

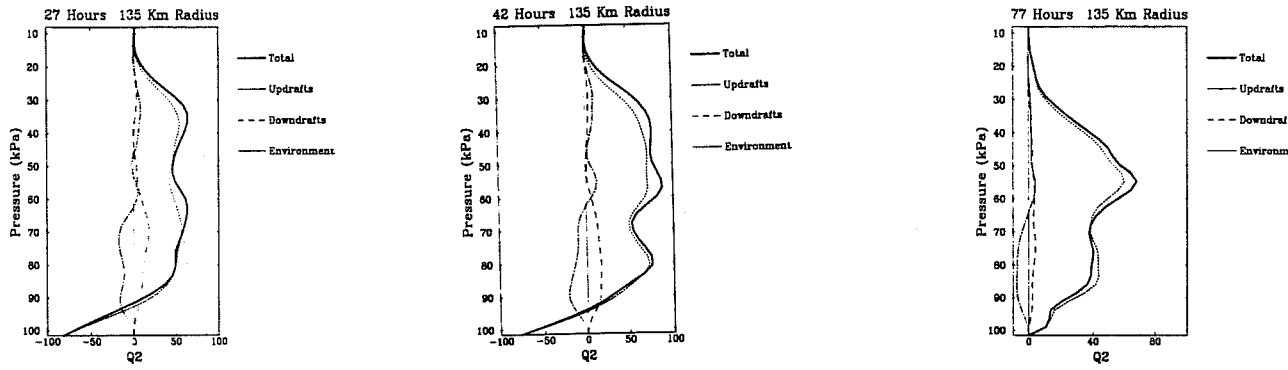


Figure 5: Apparent heat sink (Q2) over the periods shown in figure 1.

The small contributions to the heating function made within the cumulus appear to be concentrated near or above the freezing level. The downdrafts also show little contribution to the Q1. An acception is at the transition time where the downdraft showed some significant mean cooling below the melting level. It was this cooling that was attributed to the continual breakdown of the vortex prior to transition.

Figure 5 depicts the apparent moisture sink as it evolves over the genesis period and is partitioned among updrafts and downdrafts. As with Q1, Q2 is dominated by contributions from the environment where subsidence is drying. The cumulus plumes are maintaining more constant moisture levels during the moist neutral ascent. This is true, before and after transition to the deepening stage. It appears that the shape of the profile evolves somewhat across the transition stage with the drying shifted from a peak 350 mb at 24 hours, to 500-600 mb at 60 and 77 hours. Moreover, there is a tendency for low level moistening at 24 and 42 hours, which weakens by 60 hours and than disappears by 77 hours.

The reason for this behavior is better understood by considering Figure 6 which shows how Q2 breaks down among processes. There it can be seen that the low level net moisture source in the pre transition stage results from an interplay between evaporational moistening, drying from explicit subsidence and moistening or drying by vertical diffusion. The vertical diffusion term contains the effects of both evaporation from the ocean surface and mixing down from above. Following transition, this term seems to be most affected, as it becomes predominantly positive instead of negative. Two effects have occurred, first the air is more moist above and second, the magnitude of surface evaporation is increased due to the increase in storm wind intensity.

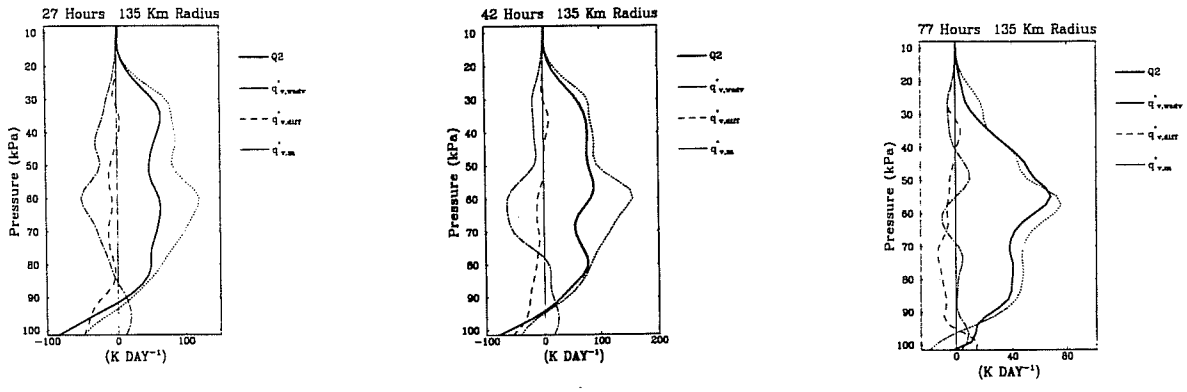


Figure 6: Apparent heat sink (Q2) broken down into contributions by processes over the periods shown in figure 1.

A persistent feature of the Q2 profile was a moisture sink from phase changes at 600 mb which was compensated by a source from upward convective transport. This was the region just below the melting layer and a region where downdrafts are locally enhanced through melting. The effect then is to provide an impetus for updraft strength to increase in response to the locally decreased stability resulting from the melting. This then enhances the updraft condensation process and the upward transport of moisture. Note that this focus of Q2 provides a secondary vertical maximum early in the storm and persists to become the primary peak in Q2 after transition and into the dissipation stage. Moreover this corresponds well to a peak in the Q1 profile which also lowers after storm transition. This suggests that the ice phase is playing a major role in shaping the vertical profile of cumulus heating.

One can combine subtract the Q2 profile and QR profile from the Q1 profile to obtain the net effect of the cumulus on the moist static energy. This calculation is displayed in Figure 7. This calculation shows the net change in moist static energy to be confined to the upper troposphere until the weakening stage when a low level increase in moist static energy occurs. This suggests that the cumulus are having the net effect of depositing energy at upper levels centered around 400 mb. Since there are no sinks below, it can be surmised that the energy is derived from local air-sea interaction and from transport across the boundaries of the inner domain. Since the effect of air-sea interaction shown in the diffusion contribution of Figure 8 was small compared to the level of heating then lateral transport must be the dominate source of moist static energy.

The small Q1-Q2-QR contribution at low levels during the mature stage is indicative of the

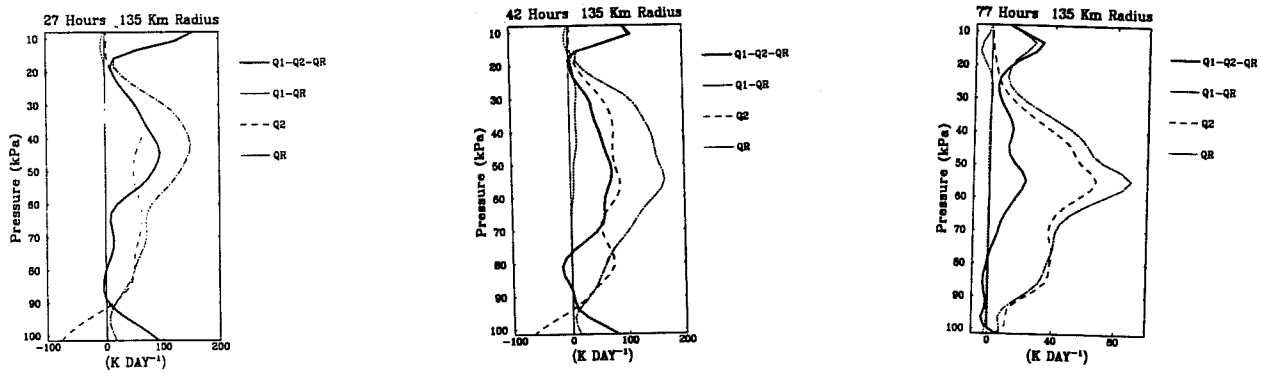


Figure 7: Q1-Q2-QR at times used in figure 1

neutral ascent where $\theta_e$ is approximately constant below 500 mb. As the water cools and the dissipation stage is entered, the large scale neutral ascent gives way to more shallow convective plumes.

# 5. Total Heating Budget

It is now of interest to examine the role played by the average vertical motion compared to the contribution by the convective scale. Figure 8 depicts the evolution of the averaged local tendency in potential temperature as it is partitioned among convective regimes. It is readily apparent that the total potential temperature change is considerably less that depicted by Q1, suggesting a strong compensatory role of the mean motions. It is apparent that the updrafts generally have negative tendencies while the downdrafts are positive. This suggests that the cumulus are in the net cooling in the region of the updraft! In fact the warming downdrafts approximately cancel that cooling so that the net domain scale tendency is best represented by the changes occurring in the environment of weak vertical motion. There the storm had net cooling prior to transition followed by less cooling to neutral conditions after transition. The high degree of variability suggests that the sign of the average potential temperature change is somewhat transient.

Figure 9 partitions the mean potential temperature change between Q1 and and the vertical transport by the mean vertical motion and mean horizontal transport. It is readily apparent that there is an approximate balance between cooling by the mean upward vertical motion in the domain and the convective scale Q1 so that the domains net temperature change is 1-2

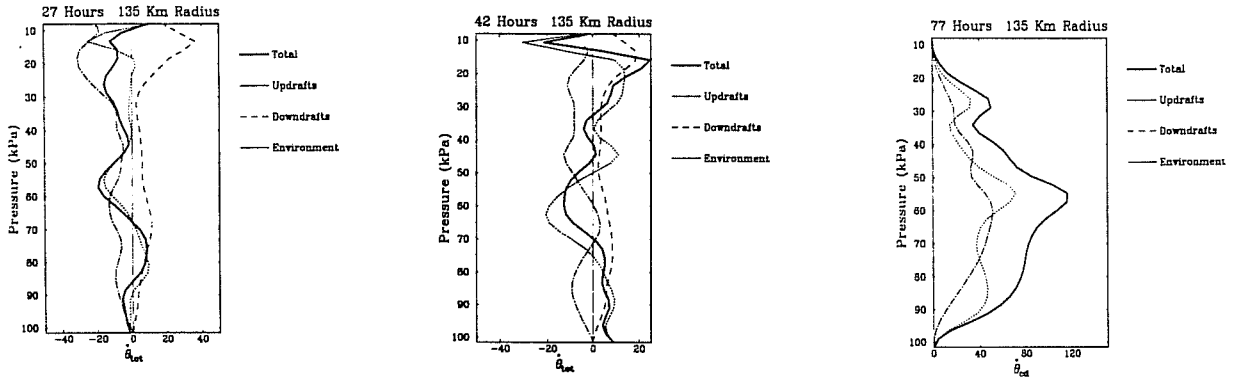


Figure 8: Averaged tendency $\theta$ at times used in figure 1

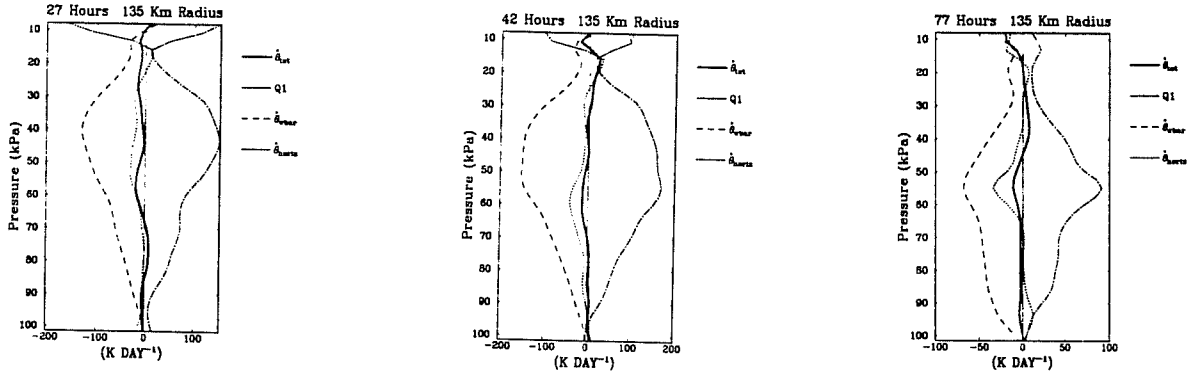


Figure 9: $\theta$ tendency partitioned among Q1 and transport at times used in figure 1

orders of magnitude less than the convective heating rates from Q1. This together suggests that the cumulus are driving a meso-$\alpha$ scale circulation which is warming far away from where the convection is occurring and more often cooling on the average in the vicinity of the convection! Hence the convective towers seem to be closely coupled to the meso-$\alpha$ scale circulation and are the manifestation of the vertical motion of that circulation! It seems that the environment experiences little net heating from the convection near the convection. This is supportive of the equilibrium assumption commonly assumed for cumulus parameterization, although the equilibrium seems to be over larger scales than one might expect.

# 6. Microphysics Contribution

A major component of the Q1 forcing is through a potential temperature tendency resulting from phase change. These include condensation and sublimation from the vapor state to a liquid or solid phase (cd), evaporation or sublimation from a vapor phase to a liquid or ice phase (ev), melting from an ice phase to a liquid phase (ml), and freezing from a liquid to the ice state (fz). The contribution to the Q1 heating at 24 hours from each of these forcings is given in figure 12. Note that the "cd" was the largest contribution to the moist tendency and was found most strong in the updraft. The peak warming by "cd" was near 600 mb. As mentioned earlier, it is expected that this level was significant because it is just below the melting level where cooling from above tends to destabilize and so enhance the updraft.

The melting induced cooling "ml" peaked at 600mb, consistent with this argument. Note that the melting effect was actually strong in the updraft as well as downdrafts. Its effective cooling reached 40 K day$^{-1}$ which is nearly a third of the magnitude of the condensation induced heating.

Warming resulting from freezing "fz" peaked at 480mb, just above the melting level. Its peak rates were 20-30 K day$^{-1}$ and is stong primarily in the updraft. Cooling by "ev" was most strong in the environment. a small amount of "ev" potential temperature forcing was calculated in the updraft at about 450 mb, attributable to evaporation of cloud water induced by the Bergeron process. A surface peak in evaporation accounts for the Q1 cooling near the surface discussed earlier. The surface peak remains even following transition although evaporation in the 3 km above the surface layer lessens after transition.??

These results demonstrate that the great majority of the phase related thermal effects are found in the updraft. There condensation/sublimation is by far the first order process while the processes of melting and freezing tend to modulate the "cd" related warming. The importance of ice to liquid phase changes are concentrated between 600-400 b as would be expected and it is these processes which define the level of peak heating during the mature system. The shape of the heating function, will be shown below, to be of consequence to the moist adiabatic production of potential vorticity.

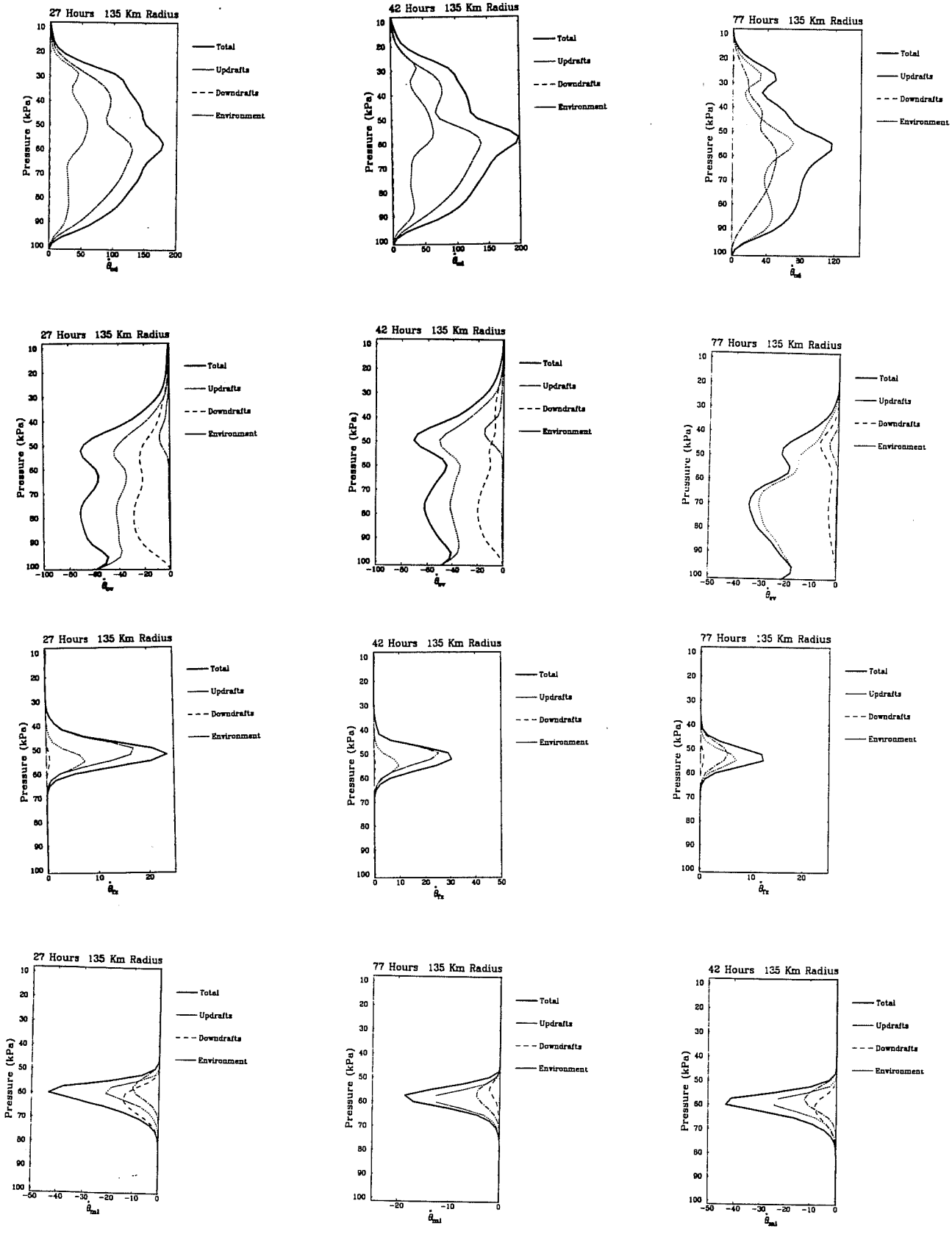


Figure 10: $\theta$ moisture tendency partitioned according to microphysical process at times used in figure 1

# 7. Potential Vorticity Forcing

Because of the greater tendency for unbalanced in the weak inertial stability of the tropics, Ertel Potential vorticity was taken to be the critical parameter characteristic of the flow and which represents the overall state of stored development. The Ertel Potential Vorticity is defined as:

$$P = -\frac{\left[\epsilon_{kij}\left(\frac{\partial u_i}{\partial x_l}\right) + f_k\right]}{\rho}\frac{\partial \theta_v}{\partial x_k}. \tag{5}$$

where $\theta_v$ is the virtual potential temperature. Ertel (1942) demonstrated that potential vorticity is invariant under dry adiabatic flow. The form of P defined above uses the virtual potential temperature to improve conservation in its application to moist flow. Hence changes in the potential vorticity anomalies associated with the developing warm core vortex, brought on by moist processes reveal important changes in the vortex structure occurring during genesis and the moist processes most responsible for those evolutionary changes.

Because of the small dynamic scale of the flow, however, it is likely impossible to invert a potential vorticity anomaly to attain a valid solution of the flow, especially in the pre genesis phase when inertial stability is low. Nevertheless, the conserved potential vorticity represents a lasting characteristic of the flow which defines the direction adjustment must take. It is for this reason that our experience modeling this event led us to the fact that the centroid of the potential vorticity anomaly was the best predictor of where new convection would form, even though its position was displaced from the transient position of lowest surface pressure before transition.

Diabatic and moist adiabatic changes to $\theta_v$ and momentum lead to the creation or destruction of potential vorticity. The effect of diabatic density variation on potential vorticity is negligible compared to the variations caused by diabatic or moist adiabatic changes in potential temperature gradient or velocity. We can then define sources of potential vorticity from Q1 as well as diabatic changes in momentum, such as friction or precipitation drag or by moist adiabatic and diabatic changes in potential temperature. The sources of $P$ can thus be expressed:

$$\dot{P} = -\frac{\left[\epsilon_{kij}\left(\frac{\partial \dot{u}_i}{\partial x_l}\right) + f_k\right]}{\rho}\frac{\partial \theta}{\partial x_k} - \frac{\left[\epsilon_{kij}\left(\frac{\partial u_i}{\partial x_l}\right) + f_k\right]}{\rho}\frac{\partial \dot{\theta}}{\partial x_k}, \tag{6}$$

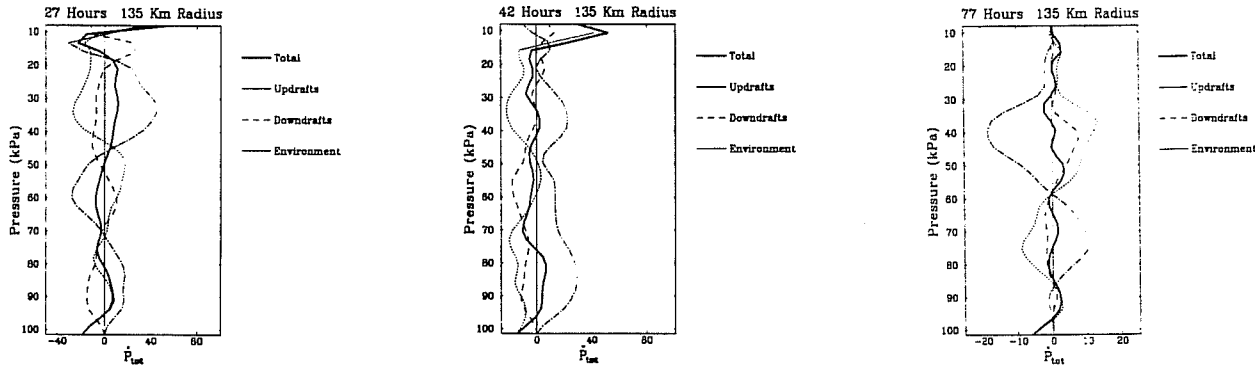


Figure 11: Potential vorticity change

where

$$\dot{u_i} = \dot{u}_{iTURB} + \dot{u}_{iPRECIPITATION\,DRAG} \tag{7}$$

and where

$$\dot{\theta} = Q1 + \dot{\theta}_{TURB} \tag{8}$$

where the turbulence terms are assumed to contain the effects of heat transfer and friction from the surface.

It is interesting to further divide the Q1 contribution to potential vorticity tendency into:

$$\dot{P}_{Q1} = \dot{P}_{VET} + \dot{P}_{Q_R} + dotP_{C^*}. \tag{9}$$

The potential vorticity tendency due to phase conversion can be itself divided as:

$$\dot{P}_{C^*} = \dot{P}_{CD} + \dot{P}_{EV} + \dot{P}_{ML} + \dot{P}_{FZ} \tag{10}$$

where CD ferers to condensation and sublimation to ice, EV represents evaporation and sublimation to vapor, ML represents melting and FZ represents freezing.

The cumulus contributions to potential vorticity forcing are given below:

# 8. Conclusions

These results demonstrate that the cumulus within the developing cluster are tightly coupled into circulations of a scale much larger than the cumulus. There seems to be little evidence

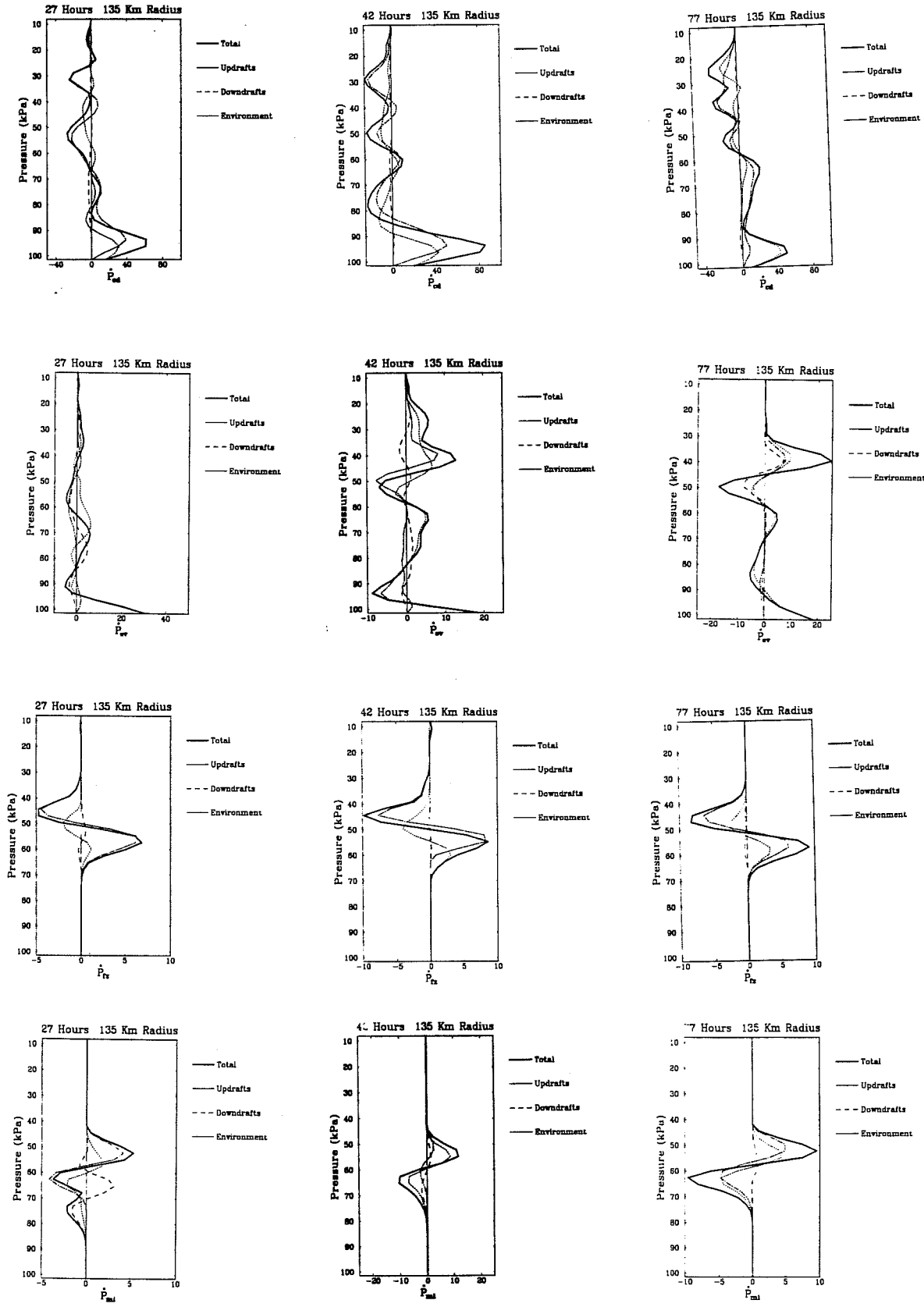


Figure 12: Potential vorticity change to to microphysical changes

that substantial subsidence is forced locally in the environment between the cumulus of the ensemble.

It is also apparent the the cumulus do not act to heat the near environment, but instead are are near the same temp[erature of the environment. The heat released by condensation is closely matched by the the expansional cooling of the rising motion. Although it has been speculated by previously by this author and others that much of the released energy of the cumulus ends up moving away from the clouds as gravity waves, there seems to be no evidence from these results to support that. Instead, the vertical upward motion in the vicinity of the cumulus in not compensated locally to a large extent, and is instead compensated by sinking motion hundreds and thousands of kilometers from the storm.

These results show that that may be true before the storm development as well as during and after. The surprising result is the degree to which the modeled convection seems to be controlled by the larger environment, despite the fact that assumptions such as those often made for a parameterization, are not made here.

# References

Chen, C. and W. R. Cotton, 1983: A one-dimensional simulation of the stratocumulus-capped mixed layer. *Bound.-Lay. Met.*, **25**, 289–321.

Cotton, W. R., M. A. Stephens, T. Nehrkorn, and G. J. Tripoli, 1982: The colorado state university three-dimensional cloud/mesoscale model - 1982. part ii: An ice phase parameterization. *J. Rech. Atmos.*, **16**(4), 295–320.

Cotton, W. R. and C. J. Tremback, 1989: The colorado state university regional atmospheric modeling system 1989: Model formulation. *Unknown.*

Ertel, H., 1942: Ein neuwr hydrodynamischer erhaltungssatz. *Die Naturwissenschaften*, **30**, 543.

Klemp, J. B. and D. K. Lilly, 1980: Mountain waves and momentum flux. In *Orographic Effects in Planetary Flows*, chapter 4, pages 116–141. GARP Publ. Ser. No. 23, ICSU/WMO. (Available from World Meteorological Organization, Case Postale No. 5, CH-1211 Geneva 20, Switzerland).

Louis, J. F., 1979: A parametric model of vertical eddy fluxes in the atmosphere. *Bound.-Lay. Met.*, **17**, 187–202.

Tremback, C. J. and R. Kessler, 1985: A surface temperature and moisture parameterization for use in mesoscale numerical models. In *Preprints, Seventh Conference on Numerical Weather Prediction, Montreal.* Amer. Met. Soc.

Tripoli, G. J., 1992: An explicit three-dimensional nonhydrostatic numerical simulation of a tropical cyclone. *Meteorol. Atmos. Phys.*, **49**, 229–254.

Tripoli, G. J., 1993: Genesis of rainbands within a tropical cyclone. In *20th Conference on hurricanes and tropical meteorology, American Meteorological Society.* San Antonio, TX.

Tripoli, G. J., 1994: Comparison of operational predictions by a nonhydrostatic model using a terrain-following vertical coordinate to those using eta-type topography. In *Tenth Conference on Numerical Weather Prediction.* Portland, Oregon (Oral Presentation).

# 9. Acknowledgments

This work was supported by a grant from the National Science foundation (ATM-9101434).Thanks to Bradd Hoggatt and Pete Pokrandt for their assistance.